PHOTOSYNTHETICA
International Journal for Photosynthesis Research

DOI 10.32615/ps.2023.018 PHOTOSYNTHETICA 61 (3): 285-296, 2023

Excess energy and photosynthesis: responses to seasonal water limitations in co-occurring woody encroachers of the semi-arid Southern Great Plains

H.D. RAUB[*,+], N. RAJAN[**], K.J. MCINNES[**], and J.B. WEST[*]

Department of Ecology and Conservation Biology, Texas A&M University, College Station, TX 77843, USA[*]
Department of Soil and Crop Sciences, Texas A&M University, College Station, TX 77843, USA[**]

Abstract

Woody plant areal encroachment is pervasive throughout the Southern Great Plains, USA. The ability of woody plants to dissipate excess solar radiation – dynamically over the day and sustained periods without recovery overnight – is key for maintaining photosynthetic performance during dry stretches, but our understanding of these processes remains incomplete. Photosynthetic performance and energy dissipation were assessed for co-occurring encroachers on the karst Edwards Plateau (*Juniperus ashei*, *Prosopis glandulosa*, and *Quercus fusiformis*) under seasonal changes in water status. Only *J. ashei* experienced mild photoinhibition from sustained energy dissipation overnight while experiencing the lowest photochemical yields, minimal photosynthetic rates, and the highest dynamic energy dissipation rates at midday during the dry period – indicating susceptibility to photosynthetic downregulation and increased dissipation under future drought regimes. Neither other encroacher experienced sustained energy dissipation in the dry period, though *P. glandulosa* did experience marked reductions in photosynthesis, photochemical yields, and increased regulatory dynamic energy dissipation.

Keywords: carbon cycling; drought avoider; drought tolerant; grasslands; nonphotochemical quenching; savannas.

Introduction

Semi-arid regions – where potential evapotranspiration exceeds precipitation – drive global interannual variation in atmospheric CO_2 due to the variable availability of water (Poulter *et al.* 2014, Ahlström *et al.* 2015). Climatic shifts in semi-arid regions will have considerable impacts on photosynthetic uptake, with the Southern Great Plains of the United States specifically predicted to experience increasing variability in productivity by 2100 (Klemm *et al.* 2020) due to increased aridity (Seager *et al.* 2018) and drought severity (Seager *et al.* 2007, Strzepek *et al.* 2010,

Highlights

- Water stress produced mild photoinhibition in juniper photosystems overnight
- Midday photochemical capacities fell and energy dissipation rose with low water status
- Juniper and mesquite experienced the greatest dissipation and reduced photochemistry

Received 3 December 2022
Accepted 18 April 2023
Published online 25 May 2023

[+]Corresponding author
e-mail: raubdh@gmail.com

Abbreviations: Chl:Car – ratio of chlorophyll to carotenoid contents; DOY – day of the year; E – transpiration rate; F_0 – minimal fluorescence yield of the dark-adapted state; F_m – maximal fluorescence yield of the dark-adapted state; F_m' – maximal fluorescence yield of the light-adapted state; F_s – steady-state fluorescence; F_v – variable fluorescence; F_v/F_m – maximal quantum yield of PSII photochemistry; g_s – stomatal conductance; NPQ – nonphotochemical quenching; P_{Nmax} – light-saturated net photosynthetic rate; VPD – vapor pressure deficit; $\Phi_{f,D}$ – quantum yield of constitutive nonregulatory NPQ; Φ_{PSII} – effective quantum yield of PSII photochemistry; $\Phi^r_{(NP)}$ – quantum yield of regulatory light-induced NPQ; ψ_{MD} – midday stem water potential; ψ_{PD} – predawn water potential.

Acknowledgments: This work was supported by the Sid Kyle Endowment from the Department of Ecology and Conservation Biology (ECCB) at Texas A&M University (TAMU), the TAMU College of Agriculture and Life Sciences Excellence Fellowship, and the TAMU ECCB Harry Wayne Springfield Graduate Assistantship. Support by AFRI grant no. 2019-68012-29819 from the USDA National Institute of Food and Agriculture is also gratefully acknowledged. Additional support for JBW was provided by the National Science Foundation.

Conflict of interest: The authors declare that they have no conflict of interest.

Cook *et al.* 2015). Climatic effects on woody plants of the Southern Great Plains are particularly concerning due to their recent areal expansion (Barger *et al.* 2011) coupled with their differential responses to water stress and drought mortality (Fensham *et al.* 2009, Choat *et al.* 2012, Moore *et al.* 2016). With water deficits and temperatures expected to increase in the future, we need a better understanding of how recent co-occurring encroachers in the semi-arid region of the Southern Great Plains will photosynthetically respond to expected water limitations and excess energy.

Absorbed light energy by chlorophyll photosystems can be dynamically quenched in three ways: (*1*) photochemically *via* photosynthesis, (*2*) fluorescence of excited chlorophyll electrons, and (*3*) photoprotective heat release of excess energy through nonphotochemical quenching (NPQ; Maxwell and Johnson 2000). Less light quenched by photosynthesis requires greater dissipation of excess energy *via* NPQ (Maxwell and Johnson 2000, Lazár 2015). The inability to dissipate excess energy creates photodamage from reactive oxidants, while photoprotective mechanisms safely quench excess energy (Demmig-Adams and Adams 2018, Malnoë 2018).

If photochemical quenching capabilities are surpassed under stressful conditions, plants may employ both dynamic and sustained forms of energy dissipation (NPQ) to protect leaves from photodamage (Malnoë 2018, Verhoeven *et al.* 2018). This is in addition to a basal constitutive NPQ that is nonregulatory in function (Lazár 2015). As dynamic stressors like excessive light, temperature, and evaporative demand increase over the day, the fraction of light used in photochemical quenching decreases due to closing reaction centers (Adams *et al.* 2008, Murchie and Lawson 2013). This controlled downregulation causes dynamic energy dissipation to increase diurnally *via* regulatory light-induced NPQ ($\Phi^{r}_{(NP)}$) as photochemical uses are surpassed. This is a photoprotective mechanism activated by proton accumulation in the thylakoid lumen in response to excess light absorption (Demmig-Adams and Adams 1996, Hendrickson *et al.* 2004). The proton accumulation induces relative shifts in the xanthophyll cycle pigments, a pool of three carotenoid pigments, to quench excess energy quickly under changing dynamic stressors before relaxing overnight (Demmig-Adams and Adams 1996, Müller *et al.* 2001, Hendrickson *et al.* 2004).

Over longer periods of stress, sustained NPQ becomes necessary which causes sustained photoinhibition of the maximal quantum yield of PSII photochemistry (F_v/F_m) which is achieved in a dark-adapted state (Verhoeven 2014, Verhoeven *et al.* 2018). Photoinhibition refers to the decreased ability to fix CO_2 relative to nonstressful conditions from photoprotective or photodamaging mechanisms (Malnoë 2018). Photoinhibition can occur seasonally due to sustained stressors like low temperatures or water limitations (Fernández-Marín *et al.* 2017) by retaining the xanthophyll cycle in an energy-dissipating state overnight (Demmig-Adams and Adams 1996). This dissipating state reduces the F_v/F_m that recovers overnight (Verhoeven 2014, Fernández-Marín *et al.* 2017, Verhoeven *et al.* 2018) which can reduce photosynthetic uptake substantially under light-limiting periods such as dawn and light-saturating conditions at midday in severe cases (Adams *et al.* 2008, Murchie and Ruban 2020). Additional carotenoid pigments have been found to dissipate excess energy by increasing in concentration during droughts, low temperatures, and chilling (Esteban *et al.* 2015, Fernández-Marín *et al.* 2017). Controlled photosynthetic downregulation is well documented in overwintering evergreens where cold environments and shorter photoperiods impede the ability to fix carbon, which induces photoprotective sustained dissipation for leaves until the spring (Verhoeven 2014). Conifers generally experience more winter-sustained energy dissipation than broadleaf trees (Míguez *et al.* 2015).

There is a paucity of studies evaluating seasonal stressors on photosynthetic and energy-dissipating strategies among major co-occurring Southern Great Plains woody encroachers. Studies have been restricted to diurnal (Liu and Guan 2012), single species (Msanne *et al.* 2017), and potted sapling experiments (Bihmidine *et al.* 2010) of related North American species. The most notable findings of seasonal responses among co-occurring encroachers come only from similar Mediterranean chaparral vegetation (Martínez-Ferri *et al.* 2000, Werner *et al.* 2002, Ain-Lhout *et al.* 2004, Baquedano and Castillo 2007, Fernández-Marín *et al.* 2017). Available studies of woody species indicate leaf traits and water status are influential with evergreens experiencing sustained photoinhibition in colder temperatures, but hot, dry periods causing sustained photoinhibition and decreased gas exchange for those with lower water status (Martínez-Ferri *et al.* 2000, Werner *et al.* 2002, Ain-Lhout *et al.* 2004, Baquedano and Castillo 2007, Barron-Gafford *et al.* 2012). A comparison of seasonal photoinhibiting responses and energy-dissipating strategies among the most prevalent co-occurring woody encroachers in North America or the Southern Great Plains does not appear to have been done – particularly without field studies of matured trees with representative rooting behaviors. This gap is concerning considering the diversity of strategies that North American encroachers possess on water-limited landscapes (Barger *et al.* 2011), which may induce differing photosynthetic responses among encroachers under drier, hotter climatic shifts in the future.

Drought-tolerant *Juniperus* spp. and drought-avoiding *Prosopis* spp. are among the greatest woody encroacher genera in western North America (Barger *et al.* 2011) but differ in both leaf traits and water-use strategies. Drought tolerators can tolerate lower water potentials by resisting embolism, and drought avoiders maintain steady water status (Wei *et al.* 2019) by minimizing transpirational water loss or maximizing water absorption with deep roots (Abobatta 2019). Oak (*Quercus* spp.) is an additional encroacher that is prevalent in locally scattered areas (Van Auken 2009). All three genera have species (*J. ashei*, *P. glandulosa*, *Q. fusiformis*) in the Southern Great Plains that co-occur on the Edwards Plateau in West-Central Texas.

Ashe juniper (*J. ashei*) is restricted mostly to the driest part of the landscape with 10–15 cm of soil above limestone bedrock (Hall 1952) – with reports of taproots

reaching 7–9 m in depth through cracks or fissures (Jackson *et al.* 1999, McElrone *et al.* 2004) – has small scale leaves, poorly controlled stomata, low stomatal densities ranging from 500 to 1,000 cm^{-2} (Johnsen 1963, Johnson *et al.* 2018a), and multi-year leaf lifespans. Live oak (*Q. fusiformis*) is a semi-evergreen drought avoider capable of rooting deep in the limestone at 22 m (Jackson *et al.* 1999) and has the largest leaves which fall off and bud anew quickly in the spring (Thyroff *et al.* 2019). Honey mesquite (*P. glandulosa*) is restricted to the deepest soils of the Edwards Plateau, though relatively shallow for the species at 1.5–2 m (Eggemeyer and Schwinning 2009), has thin leaflets, high stomatal densities ranging 11,100 to 20,000 cm^{-2}, and has the shortest leaf lifespan as a deciduous species (Meyer *et al.* 1971). Leaf-level photosynthesis and generally water status are lower in *J. ashei* (some comparable values are exhibited for *P. glandulosa* in shallow soils) than the other species (Owens 1996, Eggemeyer and Schwinning 2009, Bendevis *et al.* 2010).

The objectives here were to assess the photosynthetic responses and the energy-dissipating strategies of co-occurring encroacher genera in the semi-arid Southern Great Plains to seasonal dry periods with excess energy. Specifically, *J. ashei*, *P. glandulosa*, and *Q. fusiformis* were assessed for photoinhibitory responses during seasonal wet and dry periods with their differential access to soil moisture and leaf traits. Due to its low water status and restriction to the driest locations on the landscape, *J. ashei* was hypothesized to experience mild sustained photoinhibition and greater dynamic energy dissipation during the hot, dry summer compared to smaller responses from *Q. fusiformis* and *P. glandulosa*. Freezing temperatures were hypothesized to elicit mild photoinhibition for both overwintering species (*J. ashei* and *Q. fusiformis*).

Materials and methods

Study site, tree selection, and mobile sampling platform: The study was conducted at the Sonora Experimental Research Station (30.25873 N, 100.56799 W, 695 m above sea level) on the karst landscape of the Edwards Plateau in West-Central Texas (Fig. 1). Daily average temperatures range from 10.5–26.3°C with annual rainfall averaging 550 mm (Western Regional Climate Center 2020). The climate is considered semi-arid, and the research site is dominated by Tarrant stony and silty clays (Crawford 2017).

Five nonjuvenile individuals from each species ($n = 15$) were selected based on isolation from other trees located at least 1 m away, good leaf health, full canopies, level terrain, and accessibility for a 4-m mobile sampling ladder located on a trailer (Fig. 1S, *supplement*). Selected trees were within the average tree height classes for each species (Fortes *et al.*, unpublished) ranging from 2.8–4.2 m. Sampling was conducted equitably across species during the day to reduce temporal bias for any one species. Two sunlit leaves located apart on each tree were sampled and then averaged together to create average leaf-level values per tree. Horizontal leaves for live oak and branches of juniper were utilized, while the leaflets closest to horizontal were selected from the downwards drooping leaves of mesquite. Separate pairs of leaves were used for different physiological measurements. Monthly measurements were taken over ~3–4 d from late July 2019 to late April 2020. VPD was calculated from daily measurements of temperature and relative humidity (model *EE184*, *Campbell Scientific Inc.*, Logan, UT, USA) using the *plantecophys* package (Duursma 2019) in *RStudio version 4.0.2*, while daily precipitation was collected with a tipping-gauge rain bucket (model *TB4*, *Campbell Scientific Inc.*, Logan, UT, USA).

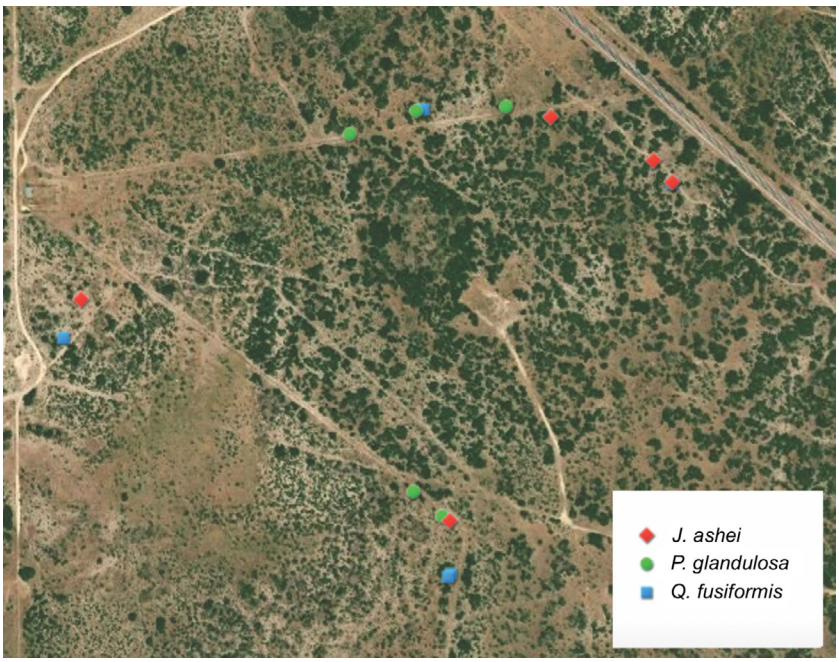

Fig. 1. Map of the study site and selected trees at the Sonora Experimental Research Station in Central Texas utilized for access by mobile sampling platform. Five individuals of each species were selected ($n = 15$) with their locations represented by *red diamonds* for *J. ashei*, *green circles* for *P. glandulosa*, and *blue squares* for *Q. fusiformis*. Two individuals for *Q. fusiformis* are located extremely close (but >1 m away) to each other at both the northern and southern locations they are depicted.

Soil depth survey: Soil depth was recorded by hammering a metal pole until an impenetrable layer was hit, similar to the prior methodology on the Edwards Plateau (Elkington *et al.* 2014). Measurements were taken in the four cardinal directions and one meter away from each tree base. A maximum of 70 cm in soil depth was measured and an average soil depth measurement per tree was created from the four subsamples.

Gas-exchange measurements: A portable gas-exchange system (model *LI-6800*, *LI-COR Biosciences*, Lincoln, NE, USA) was used to measure instantaneous gas-exchange parameters including light-saturated net photosynthetic rates (P_{Nmax}) for carbon assimilation, transpiration rates (E), and stomatal conductance (g_s). Leaves smaller than the 2 cm^2 gasket were cut and stored in wetted plastic bags for later leaf-area corrections. Projected leaf areas were scanned into *ImageJ* (*U.S. National Institutes of Health*, Bethesda, MD, USA), and all gas-exchange parameters were corrected on a one-sided leaf area basis. The *J. ashei* leaflets were debranched and the projected leaf area was multiplied by π/2 due to their 3-D structure (Cregg 1992).

Environmental parameters were set to ambient temperature and humidity, 1,500 µmol(photon) m^{-2} s^{-1} for light-saturating conditions, and 415 µmol(CO_2) mol^{-1}. Warm-up tests were conducted initially, then infrared gas analyzers were matched before each tree sampling. Three logs per leaf were taken when sample CO_2 and H_2O vapor values stabilized according to manufacturer standard recommendations. Due to the very low transpiration rates observed some months, E values between 0 and –0.0005 mol(H_2O) m^{-2} s^{-1} were set to 0.000001 mol(H_2O) m^{-2} s^{-1} for the statistical analysis due to the rates falling within the margin of error for the infrared gas analyzers and these being indistinguishable from zero.

Fluorescence measurements and calculations: Fluorescence measurements were made with a *LI-6800 Multiphase Flash Fluorometer* (*LI-COR Biosciences*, Lincoln, NE, USA) on two leaves per tree canopy. Predawn fluorescence measurements were taken with a saturated rectangular flash of 8,000 µmol(photon) m^{-2} s^{-1} to determine the minimal (F_0) and maximal (F_m) fluorescence yields of the dark-adapted state. Midday fluorescence measurements were taken immediately after gas exchange under actinic light conditions of 1,500 µmol(photon) m^{-2} s^{-1}. A multiphase saturating flash was conducted to estimate the most accurate maximal fluorescence of the light-adapted state (F_m') and steady-state fluorescence (F_s; Loriaux *et al.* 2013).

The fraction of absorbed light that is used in photochemistry if all PSII reaction centers are open under relaxed dark-adapted conditions is represented by F_v/F_m. It is used as a key indicator of sustained regulatory NPQ and photoinhibition (Lazár 2015, Verhoeven *et al.* 2018) and is calculated by (Maxwell and Johnson 2000):

$$F_v/F_m = (F_m - F_0)/F_m \quad (1)$$

Healthy leaves have values near 0.83 (Björkman and Demmig 1987) with values lower than this indicating photoinhibition (Malnoë 2018). Strong photoinhibition refers to values below 0.2, moderate photoinhibition from 0.4–0.7 (Adams *et al.* 2008), while sustained energy dissipation is considered present below 0.8 (Verhoeven 2014) which we considered the threshold for mild photoinhibition.

The effective quantum yield of PSII photochemistry (Φ_{PSII}) for a light-adapted state is calculated by:

$$\Phi_{PSII} = (F_m' - F_s)/F_m' \quad (2)$$

with Φ_{PSII} representing the actual fraction of absorbed light used for photosynthesis in lighted conditions (Lazár *et al.* 2015).

Energy partitioning estimates the fractions of absorbed light quenched by different pathways. While complex energy partitioning strategies have been developed for specific situations, the partitioning equations by Hendrickson *et al.* (2004) were used due to their simplicity and lack of lengthy measurements (Lazár 2015). These include the proportion of light energy allocated to photochemical pathways (Φ_{PSII}), the quantum yield of constitutive nonregulatory NPQ ($\Phi_{f,D}$), and the quantum yield of regulatory light-induced NPQ (Φ^r_{NP}) with the latter two calculated as:

$$\Phi_{f,D} = F_s/F_m \quad (3)$$

$$\Phi^r_{NP} = F_s/F_m' - F_s/F_m \quad (4)$$

where $\Phi_{f,D}$ represents the heat loss of both fluorescence (f) and constitutive (D) processes. Φ^r_{NP} is associated with dynamic quenching mediated by the xanthophyll cycle throughout the day, while $\Phi_{f,D}$ is a contribution of both nonregulatory thermal dissipation processes and regulatory sustained NPQ that is not further defined (Hendrickson *et al.* 2004, Lazár 2015). Consequently, F_v/F_m is more frequently used to assess changes in regulatory sustained NPQ (Lazár 2015, Verhoeven *et al.* 2018).

Pigment analyses were used to test for changing chlorophyll and carotenoid contents due to climatic stressors. Beads of dry silica gel were used to store leaves for up to three weeks in a light-free environment at room temperature to prevent pigment degradation (Esteban *et al.* 2009). Equal masses of both leaves were homogenized together with liquid nitrogen using a mortar and pestle. Pigments were extracted with 100% methanol (HPLC grade) under dim lighting before centrifuging. A methanol blank was measured before each sample in a spectrophotometer (model *Genesys 10 UV Scanning*, *Thermo Electron Scientific Instrument Corp.*, Madison, WI, USA). Equations calculating total chlorophyll and carotenoids for low-resolution spectrophotometers were calculated from Wellburn (1994) and adjusted to a molar dry mass basis [µmol g^{-1}(pigment)] using molar masses from Sims and Gamon (2002). Samples were adjusted to fall within the linear range (0.3–0.85 absorbance) of the machine (Fernández-Marín *et al.* 2018) with readings below 0.010 absorbance at 750 nm requiring greater centrifuging (Lichtenthaler 1987). The total chlorophyll

to carotenoid content (Chl:Car) reflects relative shifts in seasonal light-harvesting to dissipating capacities. Individual xanthophylls could not be resolved.

Water potential measurements: Predawn water potential (ψ_{PD}) measurements were made to indicate the soil-water availability of the tree. Midday measurements (ψ_{MD}) were used to indicate the midday water status of the tree and were measured by placing plastic bags over the leaves to bring them into equilibrium with the stem (Turner 1988) for a minimum of 15 min to stop transpirational water loss. After excising the leaves, a pressure chamber (model *1000*, *Edaphic Scientific*, Moorabbin, AUS) was used to record the pressure when water appeared at the cut end of the stem.

Statistical analysis: Gas-exchange and fluorescence logs were removed from analysis if logs had leak percentages greater than 10%, gas-exchange parameters did not achieve stability following manufacturer recommendations, or the chamber varied from set CO_2, light intensity, and fan speed levels. Individual leaves were removed from analysis if they were an outlier (± 2 SD) from the species' mean each month.

Extended linear mixed models were employed for each physiological parameter for pigments, gas exchange, water potential, and fluorescence in *R Studio version 1.3.1056* in the *nlme* package (Pinheiro *et al.* 2020). Monthly samples were treated as one traditional growing season cohort for analysis. Fixed effects included interactions with species between a day of the year (DOY) term and higher ordered DOY^2 or DOY^3 terms depending on the plotted trend with DOY being mean centered to reduce multicollinearity issues. Random intercepts were used to account for repeated measures on each tree, while random slopes for each DOY term were determined unnecessary during model selection. Heteroscedasticity was modeled with the *varIdent* variance function in the 'weights' argument to allow variance to differ for each species each month with some values fixed based on visual inspection of distributions (Pinheiro and Bates 2000). Variance parameters were checked for optimal estimation *via* the presence of positive definite confidence intervals, reasonable values, and acceptable residual plots (Gałecki and Burzykowski 2013). Model selection began with full fixed and random effects, then random effects were selected only *via Akaike*'s Information Criterion (AIC) due to the heteroscedastic residuals, followed by fixed effects selection with the maximum likelihood ratio test (Gałecki and Burzykowski 2013). Residuals for each species and the overall model were visually checked for homogenous patterns of variance and normality followed by normality checks of the random intercepts (Pinheiro and Bates 2000, Gałecki and Burzykowski 2013). Minor departures from normality were accepted as mixed models are largely robust to nonnormality (Schielzeth *et al.* 2020, Knief and Forstmeier 2021). Post-hoc analyses were performed with the *emmeans* package (Lenth *et al.* 2020) to determine differences between the species slope trends with the *emtrends* function and main effects where appropriate utilizing the *Games-Howell* procedure.

Results

Climatic conditions: The period of the highest evaporative demand occurred in late summer with daily air temperatures averaging around 28°C and maximum VPD values peaking above 5 kPa (Fig. 2). Only one

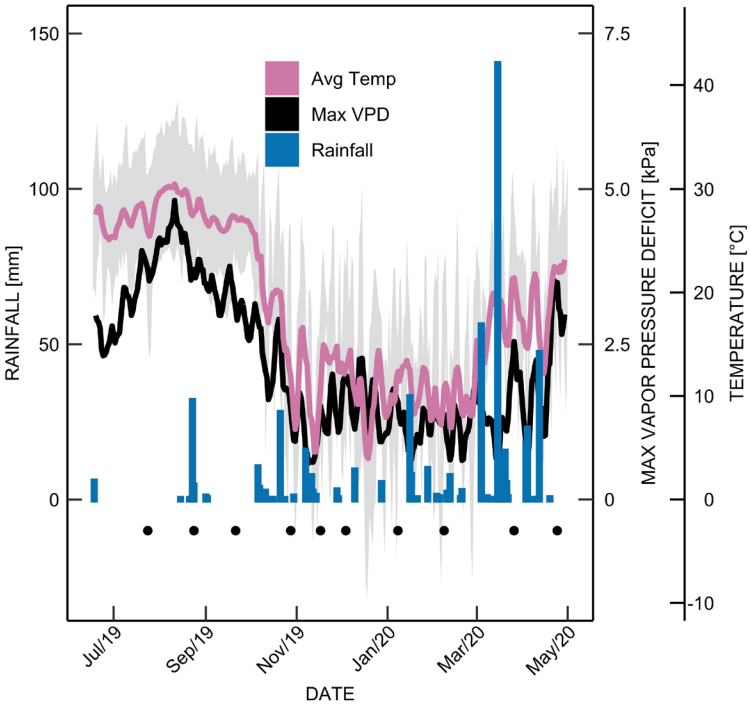

Fig. 2. Climatic conditions at the Sonora Research Station in Central Texas from June 2019 to May 2020. Total daily rainfall [mm] is shown in *blue bars*. Five-day rolling averages for average air temperature [°C] and maximum vapor pressure deficit (kPa) are shown in *pink* and *black*, respectively. Minimum and maximum daily air temperatures are shown in *grey shading*, while sampling dates are shown with *black dots*.

rain event occurred over the three months between late June to the start of October which happened during the second sampling period (Fig. 2). The total precipitation of 121 mm that fell during the summer and autumn months (July–November) was 57% below the average of 281 mm for these months from 1902–2018 (Western Regional Climate Center 2020). Winter months reached average lows of 10°C with three periods (November, January, and February) having multiple subzero (0°C) nights in the week leading up to sampling while October had one night below freezing before sampling (Fig. 2). Cumulative rainfall for winter months (December–February) was comparable to historic averages (Western Regional Climate Center 2020) with minimal amounts between late November and mid-January. March and April had four times greater rainfall than historic averages (Western Regional Climate Center 2020) with the largest events reaching values of 56, 140, and 47 mm (Fig. 2).

The ψ_{PD} and ψ_{MD} trends experienced high variability month to month and were strongly coupled to each other from summer to fall with some divergence among species occurring over winter. Both *J. ashei* and *P. glandulosa* declined in ψ_{PD} from –1.7 and –0.8 MPa in July to their lowest averages of –4.3 and –2.3 MPa respectively by mid-September, while *Q. fusiformis* consistently hovered near ~1 MPa until spring (Fig. 3*A*). Rain events in autumn led to quick responses by *P. glandulosa* and *J. ashei* by increasing ψ_{PD} to ~ –1 MPa, while *J. ashei* was the only evergreen to experience a decline during the dry January to –2.7 MPa. All species peaked in the spring for ψ_{PD} with values near –0.5 MPa. The large decreases in ψ_{PD} during the multiple dry periods produced a significantly different cubic trend between only *J. ashei* and *Q. fusiformis* (Table 1). Overall trends for ψ_{MD} among species were not significantly different (Table 1). All species declined during the summer period, rebounded with autumn rains with a slight decline in December, before peaking in the spring near –1.5 MPa for all species (Fig. 3*B*). Only *J. ashei* decreased through the dry January to –3.0 MPa. The dry period in late summer did show a marked difference between species with *J. ashei* reaching the lowest ψ_{MD} of all species at –5.1 MPa, followed by *P. glandulosa* at –4.0 MPa, and *Q. fusiformis* at –2.8 MPa (Fig. 3*B*).

Soil depth: Average soil depth was the lowest for locations with *P. glandulosa* at 48 cm (27–70 cm) over *J. ashei* at 41 cm (28–66 cm) and *Q. fusiformis* at 40 cm (31–45 cm) though these depths were not significantly different. Maximum soil depths for *P. glandulosa* were underestimated for some individuals due to the sampling technique being restricted to measuring 70 cm in depth.

Seasonal gas-exchange and pigment trends: Variability in P_{Nmax} was high among species month to month with overall DOY^2 trends significantly different between *P. glandulosa* and the other two species (both $p<0.02$; Table 1, Fig. 4*A*). Late summer produced the highest rates for *P. glandulosa* and *Q. fusiformis*, while *J. ashei* peaked during the wetter November and spring months up to 4.83 µmol m^{-2} s^{-1}. The highest P_{Nmax} of all species was exhibited by *P. glandulosa* at 20.9 µmol m^{-2} s^{-1} in July before declining 46% during the dry period in August. The decline continued through November to 5.78 µmol m^{-2} s^{-1} as leaf-drop occurred, temperatures cooled, and daylight decreased (Fig. 4*A*). P_{Nmax} hovered near ~2 µmol m^{-2} s^{-1} for *J. ashei* most months with it recording the lowest levels of all species in July and August at 0.66 µmol m^{-2} s^{-1} and 0.89 µmol m^{-2} s^{-1}, respectively. Overall, P_{Nmax} for *J. ashei* was significantly lower than for *Q. fusiformis* (Table 1) and lower than *P. glandulosa* for all months except shortly after budburst. Little variation occurred in *Q. fusiformis* with values recorded near ~12.5 µmol m^{-2} s^{-1} in the summer and ~10 µmol m^{-2} s^{-1} thereafter (Fig. 4*A*).

The *E* trends for all species declined from summer to winter before peaking in spring but were significantly different in the degree they were affected (all $p<0.03$; Table 1, Fig. 4*B*) with *P. glandulosa* showing the sharpest swings and the mildest trend occurring in *J. ashei*. July to August produced a 19% decline in *E* from 3.85 mmol m^{-2} s^{-1} for *P. glandulosa*, while *J. ashei* declined from 0.61 to 0.29 mmol m^{-2} s^{-1} through September. Spring brought peak *E* for all species with 1.9 mmol m^{-2} s^{-1}

Table 1. Extended linear mixed model outputs for gas-exchange and water-potential parameters from which posthoc analyses were performed to determine differences in seasonal trends. *P*-values less than or equal to 0.05 (*), 0.01 (**), or 0.001 (***) are shown in bold. Unused predictors indicated by NA. DOY – day of the year; *E* – transpiration rate; g_s – stomatal conductance; P_{Nmax} – light-saturated net photosynthetic rate; ψ_{MD} – midday stem water potential; ψ_{PD} – predawn water potential.

Predictor	ψ_{PD}		ψ_{MD}		P_{Nmax}		*E*		g_s	
	F-value	df(n,d)	F-value	df(n,d)	F-value	df(n,d)	F-value	df(n,d)	F-value	df(n,d)
Intercept	**497.9*****	1, 114	**4,824*****	1, 116	**254.3*****	1, 116	**419.4*****	1, 116	**177*****	1, 113
Species	1.2	2, 12	**11.4****	2, 12	**60.3*****	2, 12	**91.6*****	2, 12	**27.3*****	2, 12
DOY	**168*****	1, 114	**40.7*****	1, 116	0.5	1, 116	**34.8*****	1, 116	**20*****	1, 113
DOY^2	**57*****	1, 114	**29.6*****	1, 116	0.7	1, 116	**6.5***	1, 116	**4***	1, 113
DOY^3	**126.7*****	1, 114	**140.1*****	1, 116	NA	NA	NA	NA	**16.6*****	1, 113
Species × DOY	7**	2, 114	**40.6*****	2, 116	**4.6***	2, 116	**8.9*****	2, 116	**11*****	2, 113
Species × DOY^2	2.9	2, 114	0.3	2, 116	**6.7****	2, 116	**16.3*****	2, 116	**24.8*****	2, 113
Species × DOY^3	**18.9*****	2, 114	NA	NA	NA	NA	NA	NA	**4.5***	2, 113

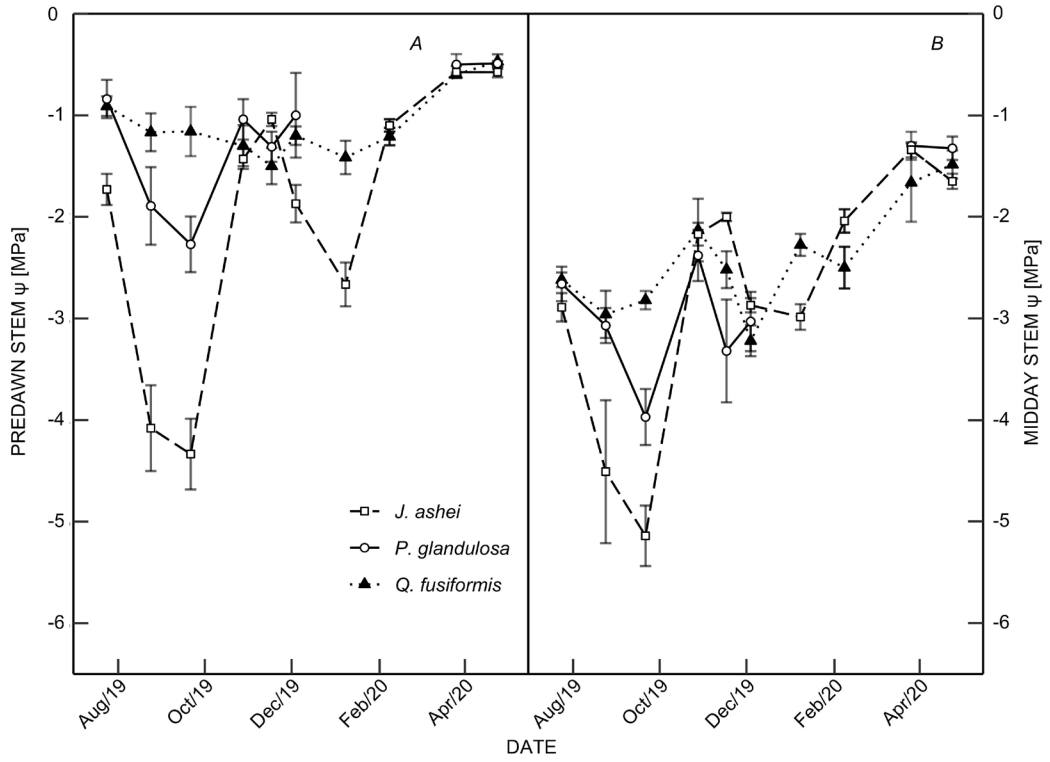

Fig. 3. Seasonal predawn (*A*) and midday (*B*) water potentials [MPa] for *J. ashei* (*dashed squares*), *P. glandulosa* (*solid lined circles*), and *Q. fusiformis* (*dotted triangles*). Data was unavailable for *P. glandulosa* during the leaf-off period of January and February. Data are expressed as means ± 1 SE (n = 15).

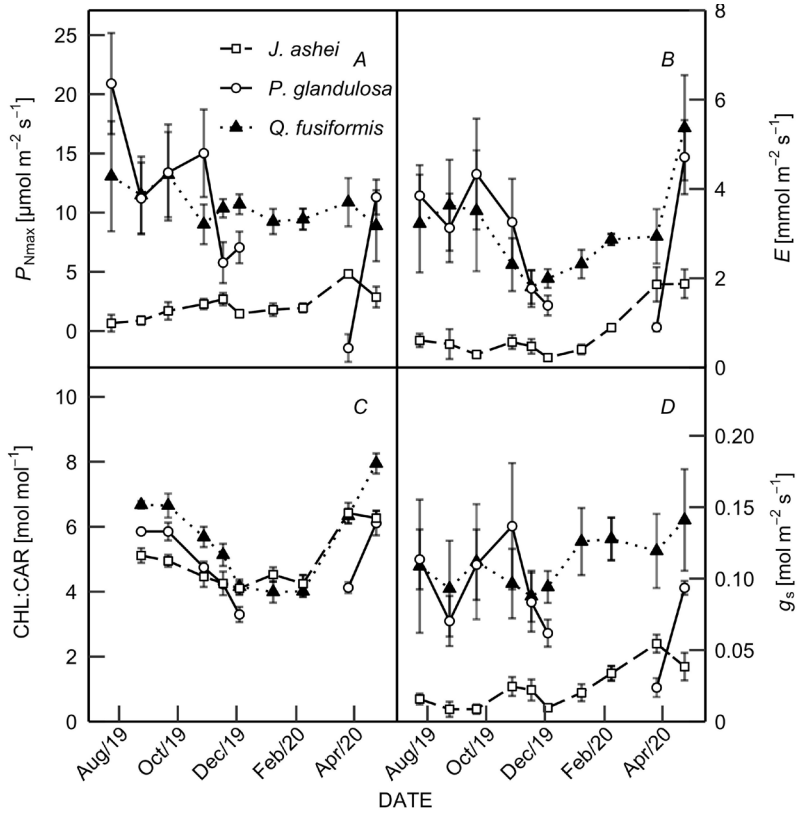

Fig. 4. Seasonal trends from 2019 to 2020 of (*A*) the light-saturated net photosynthetic rate (P_{Nmax}), (*B*) transpiration rate (E), (*C*) the chlorophyll to carotenoid ratio of pigment (Chl:Car), and (*D*) the stomatal conductance rate (g_s) among species (*J. ashei – dashed squares*; *P. glandulosa – solid lined circles*; and *Q. fusiformis – dotted triangles*). Data was unavailable for *P. glandulosa* during the leaf-off period of January and February. Data are expressed as means ± 1 SE (n = 15).

for *J. ashei*, 4.71 mmol m^{-2} s^{-1} for *P. glandulosa*, and 5.37 mmol m^{-2} s^{-1} for *Q. fusiformis*. While *E* and g_s trends were more tightly coupled to each other in *J. ashei* and *P. glandulosa*, some stronger divergence occurred in *Q. fusiformis* (Fig. 4*D*). Warm and high VPD months yielded high values of *E* for *Q. fusiformis* at 3.63 mmol m^{-2} s^{-1} while g_s varied little throughout the season at ~0.1 mol m^{-2} s^{-1} and increased slightly during the spring. The g_s trends significantly differed between *P. glandulosa* and the other two species with larger swings surrounding leaf budding and senescence (both $p<0.02$; Table 1). The overall *E* and g_s averages for *J. ashei* were significantly lower than for *Q. fusiformis* (both $p<0.0003$; Table 1) and lower than *P. glandulosa* for all months except shortly after budburst. The Chl:Car declined across species from summer to winter lows before peaking in the spring. The Chl:Car trend was significantly milder in *J. ashei* than the other two species which experienced larger transitional changes (Table 1, Fig. 4*C*). Peak values recorded in the spring were the highest in *Q. fusiformis* at 7.95 mol mol^{-1} followed by *J. ashei* at 6.42 mol mol^{-1} and *P. glandulosa* at 6.11 mol mol^{-1}. August values of Chl:Car were 20.4 and 16.0% lower than spring highs for *J. ashei* and *Q. fusiformis*, respectively, while *P. glandulosa* was only 4.26% lower. The lowest Chl:Car of all species was recorded at 3.30 mol mol^{-1} for *P. glandulosa* in December before leaf-off with winter lows for *J. ashei* and *Q. fusiformis* reaching ~4 mol mol^{-1}.

Seasonal photoinhibition trends: Seasonal F_v/F_m trends significantly differed only between *P. glandulosa* and the other two species with its rapid changes during late fall and after bud burst (Table 2, Fig. 5*A*). Isolating just the late summer period, some mild photoinhibition was induced only in *J. ashei* (F_v/F_m = 0.75) while *P. glandulosa* and *Q. fusiformis* maintained values above 0.80. Mild to moderate photoinhibition was recorded for all three species from the freezing night in October with *P. glandulosa* declining in F_v/F_m from 0.83 to 0.68. The two evergreens maintained values below 0.75 throughout the winter months and showed the greatest photoinhibition when multiple freezing nights led up to sampling during November, January, and February. Only one month of multiple freezing nights preceding sampling was experienced by *P. glandulosa* in November, which led to the lowest F_v/F_m recorded among species at 0.53. The lowest F_v/F_m for *J. ashei* was recorded in the slightly water-limited but freezing January.

Energy partition analysis: Seasonal Φ_{PSII} trends differed for all species with each experiencing reductions from July to August. A significant species and DOY^3 interaction (Table 2) was observed only in *J. ashei* where Φ_{PSII} declined to the lowest of all species at 4% during August, before increasing during autumn rains, decreasing in January, before peaking in March at 26% (Fig. 5*B*). The DOY^2 trends of Φ_{PSII} significantly differed between *P. glandulosa* and *Q. fusiformis* (Table 2) where both declined from summer peaks to winter lows before increasing again in the spring. The Φ_{PSII} for *P. glandulosa* declined from 42% in July to a low of 10% in December, while *Q. fusiformis* declined from 31% in July to a low of 14% experienced throughout winter.

Declines in Φ_{PSII} led to inverse increases in $\Phi^r_{(NP)}$ or $\Phi_{f,D}$. The $\Phi^r_{(NP)}$ among species (Fig. 5*D*) exhibited significant cubic trends (Table 1) that increased during warm, dry periods for *J. ashei* and *P. glandulosa* in addition to the end of leaf lifespan for the latter. The DOY^3 trend of $\Phi^r_{(NP)}$ for *J. ashei* peaked during August at the highest among species at 84% with lows in autumn and spring near 48%. This significantly differed from the *Q. fusiformis* trend ($p<0.0004$), which varied little and showed moderate energy dissipated by $\Phi^r_{(NP)}$ consistently near ~50%. The $\Phi^r_{(NP)}$ for *P. glandulosa* was the lowest recorded among species and occurred in July at 24% with an increase to 51% by September and a peak of 59% in December. The $\Phi_{f,D}$ trends were quadratic (Table 2) with peaks occurring during freezing periods (October, November, and January) and lows in the spring and summer (Fig. 5*C*). Peak $\Phi_{f,D}$ was the highest among species in *P. glandulosa*

Table 2. Extended linear mixed model outputs for fluorescence and pigment parameters from which posthoc analyses were performed to determine differences in seasonal trends. *P*-values less than or equal to 0.05 (*), 0.01 (**), or 0.001 (***) are shown in bold. Unused predictors indicated by NA. A variance function for the Chl:Car parameter was not required to resolve heteroscedasticity. Chl:Car – ratio of chlorophyll to carotenoid contents; DOY – day of the year; F_v/F_m – maximal quantum yield of PSII photochemistry; $\Phi_{f,D}$ – quantum yield of constitutive nonregulatory NPQ; Φ_{PSII} – effective quantum yield of PSII photochemistry; $\Phi^r_{(NP)}$ – quantum yield of regulatory light-induced NPQ.

Predictor	F_v/F_m		Φ_{PSII}		$\Phi_{f,D}$		$\Phi^r_{(NP)}$		Chl:Car	
	F-value	df(n,d)	F-value	df(n,d)	F-value	df(n,d)	F-value	df(n,d)	F-value	df(n,d)
Intercept	**157,197.9*****	1, 117	**866.9*****	1, 113	**2,664.6*****	1, 117	**9,328*****	1, 109	**5,309.9*****	1, 100
Species	**42.9*****	2, 12	**51.5*****	2, 12	**70.4*****	2, 12	**182.2*****	2, 12	**8.9****	2, 12
DOY	**101.4*****	1, 117	**22.8*****	1, 113	**13*****	1, 117	**5.7***	1, 109	**5.1***	1, 100
DOY^2	**261.4*****	1, 117	**39.9*****	1, 113	**19.7*****	1, 117	0.1	1, 109	198.1***	1, 100
DOY^3	NA	NA	**4.3***	1, 113	NA	NA	**4.7***	1, 109	NA	NA
Species × DOY	**37.4*****	2, 117	**7.2****	2, 113	**25.2*****	2, 117	**15.3*****	2, 109	7**	2, 100
Species × DOY^2	**43*****	2, 117	**72.1*****	2, 113	NA	NA	**6.6****	2, 109	10.4***	2, 100
Species × DOY^3	NA	NA	**13.1*****	2, 113	NA	NA	**8.1*****	2, 109	NA	NA

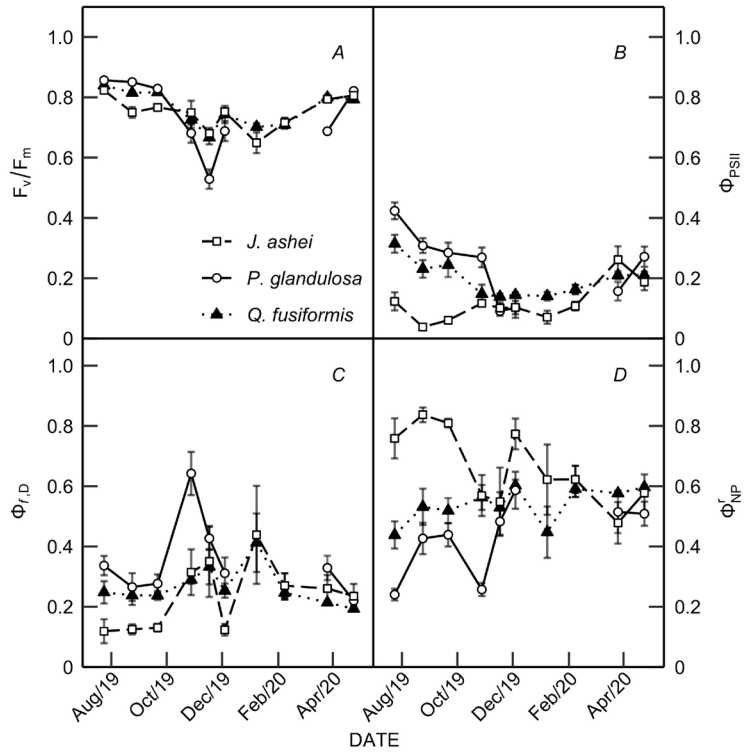

Fig. 5. Seasonal trends among *J. ashei* (*dashed squares*), *P. glandulosa* (*solid line circles*), and *Q. fusiformis* (*dotted triangles*) for: (*A*) the maximal quantum yield of photochemistry (F_v/F_m), (*B*) the effective quantum yield of PSII photochemistry (Φ_{PSII}), (*C*) the quantum yield of constitutive nonregulatory NPQ ($\Phi_{f,D}$), and (*D*) the quantum yield of regulatory light-induced NPQ ($\Phi^r_{(NP)}$). Data was unavailable for *P. glandulosa* during the leaf-off period of January and February. Data are expressed as means ± 1 SE (n = 15).

when it increased from 28 to a 64% peak during the one-night freezing period in October. Increases in $\Phi_{f,D}$ for *J. ashei* occurred after experiencing multiple freezing nights during November and January at a maximum of 44%. Little variation occurred in *Q. fusiformis* with $\Phi_{f,D}$ near 25% throughout the period except for a spike to 41% in January.

Discussion

Woody expansion is pervasive throughout the semi-arid regions of the Southern Great Plains with varying functional traits observed among encroachers (Van Auken 2009, Barger *et al.* 2011). However, little is known about how various encroachers will photosynthetically and energetically respond to increased aridity and drought severity (Seager *et al.* 2007, Strzepek *et al.* 2010, Cook *et al.* 2015). Evaluating the effects of seasonal stress among three co-occurring encroachers that vary in soil water access and leaf persistence in the semi-arid regions of Southern Great Plains is key to understanding their potential responses to these climatic shifts – particularly for the drought-tolerant *Juniperus*.

Water availability in this study was particularly limited which allowed for strong comparisons between the woody encroachers in their light-quenching strategies and photosynthetic capabilities under drier conditions. Rains over the summer and autumn were 57% below average (Western Regional Climate Center 2020) leading to ψ_{PD} that were lower (Bendevis *et al.* 2010, Elkington *et al.* 2014) or as low as past seasonal studies (Eggemeyer and Schwinning 2009, Johnson *et al.* 2018a,b). These greater water limitations caused >50% lower stomatal conductance values for *J. ashei* and *Q. fusiformis*, and average to lower transpiration rates across species compared to past studies (Owens and Schreiber 1992, Eggemeyer and Schwinning 2009, Bendevis *et al.* 2010). Peak Chl:Car in the wet spring for *J. ashei* and *Q. fusiformis* indicated a shift towards maximizing light harvesting, while the dry summer was shifted towards increased energy dissipation with lower Chl:Car (Esteban *et al.* 2015). All species were shifted towards their highest energy dissipation and lowest light-harvesting capabilities over the winter with low Chl:Car values.

Relative differences in water status were partially explained by known rooting behaviors and related water access, but the recorded soil depths provided some inconsistencies. Though the soil depth of *Q. fusiformis* was not significantly deeper (40 cm) than the other species, its higher ψ_{PD} indicated more stable water access. This stability may have been aided by its ability to root very deep through cracks or fissures in the limestone and its ability to take up water at greater depths (Jackson *et al.* 1999, McElrone *et al.* 2004). Recorded soil depths in *P. glandulosa* and *J. ashei* were more consistent with their known rooting depths, water access, and expected responses during dry periods. A soil depth of 48 cm (likely underestimated from the sampling technique) is shallow for *Prosopis* sp. (Wilson *et al.* 2001, Lombardini and Rossi 2019) but consistent with *P. glandulosa*'s apparent preferential association with the deeper pockets of soil on the Edwards Plateau (Eggemeyer and Schwinning 2009). Deeper soils on the Edwards Plateau are suggested to hold more water at depth for the same species (Elkington *et al.* 2014) which may have allowed for relatively higher ψ_{PD} in *P. glandulosa* than *J. ashei* but

still allowed responsiveness to water limitations in the relatively shallow soils for the species itself (Eggemeyer and Schwinning 2009). The high responsiveness of ψ_{PD} to water limitations in *J. ashei* and its shallow soil depth (40 cm) is consistent with its known rooting depth in the area (Hall 1952, Thurow and Hester 1997).

As hypothesized, the water limitations in *J. ashei* produced the greatest need for energy dissipation among species which reduced photosynthetic capacities. Consequently, during the dry period in late summer the drought-tolerant *J. ashei* experienced the lowest photochemical yields at midday (4% for Φ_{PSII}), lowest P_{Nmax} at 0.66–0.89 μmol m^{-2} s^{-1}, the highest dynamic energy dissipation (84% for $\Phi^{r}_{(NP)}$), the lowest ψ_{MD} below –4 MPa, and it was the only species to exhibit mild photoinhibition with F_v/F_m dropping from 0.82 in July to 0.75 (Fig. 5*A*). Reductions in F_v/F_m can substantially constrain P_{Nmax} during light-limited periods early in the day (Adams *et al.* 2008, Murchie and Ruban 2020), which indicates the mild photoinhibition here would likely show additional constraints on photosynthetic activity for *J. ashei* early in the morning; though, lack of early P_{Nmax} measurements could not confirm this. The drops in F_v/F_m in *J. ashei* in late summer are consistent with findings in *J. virginiana* in the Nebraska sandhills (Msanne *et al.* 2017) and less severe than reductions in *J. phoenicea* in Mediterranean climates (Werner *et al.* 2002). Findings here indicate that the drought-tolerant *Juniperus* species was the most photochemically constrained encroacher with reductions stretching from both light-limiting to light-saturating periods of the day during the hot, dry periods with increases in regulatory dynamic and sustained energy dissipation.

Rooted in the relatively shallow soils of the Edwards Plateau, *P. glandulosa* exhibited increases in dynamic energy dissipation and photochemical reduction but without the presence of sustained energy dissipation during the dry period. During peaks in air temperature and VPD near midday, *P. glandulosa* experienced substantial declines in P_{Nmax} (48% reduction), the most responsive increase in dynamic energy dissipation from 24 to 51%, and the largest decline in Φ_{PSII} from 42 to 31%. The reduction in photosynthetic capacities at midday for *P. glandulosa* has been exhibited before after sustained dry periods in late summer, though it only appeared after repeated periods of low water status without any notable drops (Eggemeyer and Schwinning 2009). The water limitations here appeared to have little effect on increasing sustained energy dissipation and recovery of photosystems overnight with no notable photoinhibition incurred. Minimal changes in dynamic and sustained energy dissipation were observed by *Q. fusiformis* during this period.

Photoinhibition from freezing conditions is well documented for many overwintering species (Verhoeven 2014), but it was surprising that *J. ashei* experienced peak P_{Nmax} at midday during the cool-wet period from late fall to early spring. Cooler temperatures, greater water availability, and the earlier peak of Chl:Car during this period likely allowed for higher Φ_{PSII} and midday P_{Nmax} for the drought-tolerant *J. ashei*, while *P. glandulosa* and *Q. fusiformis* had higher rates in the summer. These temporally separated peaks for *J. ashei* and *Q. fusiformis* are somewhat similar to patterns recorded by Owens (1996) and Bendevis *et al.* (2010) in these systems. The slightly higher Φ_{PSII} and the midday P_{Nmax} found here and in the prior studies (Owens 1996, Bendevis *et al.* 2010) may indicate this period provides preferable conditions for midday net photosynthetic uptake for *J. ashei* due to less severe temperature, water availability, and VPD constraints at midday. Some evidence of photosynthetic increases in other conifer species (*Pinus halpensis*) has been recorded in the similarly cool but infrequently freezing winters of Mediterranean systems relative to summer (Werner *et al.* 2002).

Conclusions: The goal of this study was to compare photosynthetic and energy-dissipating strategies of co-occurring woody encroachers in the Southern Great Plains to determine their potential responses to a changing climate. Trees likely to experience the greatest water stress suffered the greatest photosynthetic reductions and the greatest need for excess energy dissipation through regulatory pathways. The greatest impacts from hot, dry periods on photochemical capabilities affected *J. ashei* which experienced mild photoinhibition due to sustained energy dissipation, greatest dynamic energy dissipation, minimal Φ_{PSII} values (4%), and minimal P_{Nmax} recorded (0.66–0.89 μmol m^{-2} s^{-1}) during the dry summer period. This evidence suggests that *Juniperus* may be the most likely to experience declining leaf-level photosynthetic C gain over the day during the dry season, while *Prosopis* individuals in relatively shallow soils appear additionally likely to experience substantial declines in photosynthetic rates at midday. It should be noted that seasonal photosynthetic downregulation is not always to the detriment of the plant and may be indicative of beneficial photoprotective strategies, but the long-term success of these seasonal strategies is beyond the scope of this study. In contrast, the cool, wet period from late fall to early spring may provide optimal photosynthetic conditions at midday for *Juniperus* as it achieved peak P_{Nmax} compared to the other species which peaked in summer. Freezing periods resulted in moderate photoinhibition of F_v/F_m for all species. With increased aridity (Seager *et al.* 2018) and drought severity (Seager *et al.* 2007, Strzepek *et al.* 2010, Cook *et al.* 2015) predicted to increase in the future, the evidence here indicates *Juniperus* and shallowly rooted *Prosopis* on the Edwards Plateau may be particularly susceptible to photosynthetic downregulation during dry periods.

References

Abobatta W.F.: Drought adaptive mechanisms of plants – a review. – Adv. Agr. Environ. Sci. **2**: 42-45, 2019.

Adams W.W., Zarter C.R., Mueh K.E. *et al.*: Energy dissipation and photoinhibition: a continuum of photoprotection. – In: Demmig-Adams B., Adams W.W., Matoo A.K. (ed.): Photoprotection, Photoinhibition, Gene Regulation, and Environment. Pp. 49-64. Springer, Dordrecht 2008.

Ahlström A., Raupach M.R., Schurgers G. *et al.*: The dominant

role of semi-arid ecosystems in the trend and variability of the land CO_2 sink. – Science **348**: 895-899, 2015.

Ain-Lhout F., Díaz Barradas M.C., Zunzunegui M. *et al.*: Seasonal differences in photochemical efficiency and chlorophyll and carotenoid contents in six Mediterranean shrub species under field conditions. – Photosynthetica **42**: 399-407, 2004.

Baquedano F.J., Castillo F.J.: Drought tolerance in the Mediterranean species *Quercus coccifera, Quercus ilex*, *Pinus halepensis*, and *Juniperus phoenicea*. – Photosynthetica **45**: 229-238, 2007.

Barger N.N., Archer S.R., Campbell J.L. *et al.*: Woody plant proliferation in North American drylands: A synthesis of impacts on ecosystem carbon balance. – J. Geophys. Res.-Biogeo. **116**: G00K07, 2011.

Barron-Gafford G.A., Scott R.L., Jenerette G.D. *et al.*: Temperature and precipitation controls over leaf- and ecosystem-level CO_2 flux along a woody plant encroachment gradient. – Glob. Change Biol. **18**: 1389-1400, 2012.

Bendevis M.A., Owens M.K., Heilman J.L., McInnes K.J.: Carbon exchange and water loss from two evergreen trees in a semiarid woodland. – Ecohydrology **3**: 107-115, 2010.

Bihmidine S., Bryan N.M., Payne K.R. *et al.*: Photosynthetic performance of invasive *Pinus ponderosa* and *Juniperus virginiana* seedlings under gradual soil water depletion. – Plant Biol. **12**: 668-675, 2010.

Björkman O., Demmig B.: Photon yield of O_2 evolution and chlorophyll fluorescence characteristics at 77 K among vascular plants of diverse origins. – Planta **170**: 489-504, 1987.

Choat B., Jansen S., Brodribb T.J. *et al.*: Global convergence in the vulnerability of forests to drought. – Nature **491**: 752-755, 2012.

Cook B.I., Ault T.R., Smerdon J.E.: Unprecedented 21st century drought risk in the American Southwest and Central Plains. – Sci. Adv. **1**: e1400082, 2015.

Crawford M.: Refined soil data of the Texas A&M AgriLife Research Station at Sonora [Data file]. Conducted by Texas A&M Natural Resources Institute, 2017. *Retrieved from*: https://www.arcgis.com/home/item.html?id=893dbd17cf094aa1a10e6c61e8ada6d3, 2019.

Cregg B.M.: Leaf area estimation of mature foliage of *Juniperus*. – Forest Sci. **38**: 61-67, 1992.

Demmig-Adams B., Adams W.W.: The role of xanthophyll cycle carotenoids in the protection of photosynthesis. – Trends Plant Sci. **1**: 21-26, 1996.

Demmig-Adams B., Adams W.W.: An integrative approach to photoinhibition and photoprotection of photosynthesis. – Environ. Exp. Bot. **154**: 1-3, 2018.

Duursma R.: Package '*plantecophys*'. R package version 1.4-4. *Available at*: https://cran.r-project.org/web/packages/plantecophys/index.html, 2019.

Eggemeyer K.D., Schwinning S.: Biogeography of woody encroachment: Why is mesquite excluded from shallow soils? – Ecohydrology **2**: 81-87, 2009.

Elkington R.J., Rebel K.T., Heilman J.L. *et al.*: Species-specific water use by woody plants on the Edwards Plateau, Texas. – Ecohydrology **7**: 278-290, 2014.

Esteban R., Balaguer L., Manrique E. *et al.*: Alternative methods for sampling and preservation of photosynthetic pigments and tocopherols in plant material from remote locations. – Photosynth. Res. **101**: 77-88, 2009.

Esteban R., Barrutia O., Artetxe U. *et al.*: Internal and external factors affecting photosynthetic pigment composition in plants: A meta-analytical approach. – New Phytol. **206**: 268-280, 2015.

Fensham R.J., Fairfax R.J., Ward D.P.: Drought-induced tree death in savanna. – Glob. Change Biol. **15**: 380-387, 2009.

Fernández-Marín B., García-Plazaola J.I., Hernández A., Esteban R.: Plant photosynthetic pigments: Methods and tricks for correct quantification and identification. – In: Sánchez-Moreiras A., Reigosa M. (ed.): Advances in Plant Ecophysiology Techniques. Pp. 29-51. Springer, Cham 2018.

Fernández-Marín B., Hernández A., Garcia-Plazaola J.I. *et al.*: Photoprotective strategies of Mediterranean plants in relation to morphological traits and natural environmental pressure: A meta-analytical approach. – Front. Plant Sci. **8**: 1051, 2017.

Gałecki A., Burzykowski T.: Linear mixed-effects models using R. Springer, New York 2013.

Hall M.T.: Variation and hybridization in *Juniperus*. – Ann. Mo. Bot. Gard. **39**: 1-64, 1952.

Hendrickson L., Furbank R.T., Chow W.S.: A simple alternative approach to assessing the fate of absorbed light energy using chlorophyll fluorescence. – Photosynth. Res. **82**: 73-81, 2004.

Jackson R.B., Moore L.A., Hoffmann W.A. *et al.*: Ecosystem rooting depth determined with caves and DNA. – PNAS **96**: 11387-11392, 1999.

Johnsen Jr. T.N.: Anatomy of scalelike leaves of Arizona junipers. – Bot. Gaz. **124**: 220-224, 1963.

Johnson D.M., Berry Z.C., Baker K.V. *et al.*: Leaf hydraulic parameters are more plastic in species that experience a wider range of leaf water potentials. – Funct. Ecol. **32**: 894-903, 2018a.

Johnson D.M., Domec J.C., Berry Z.C. *et al.*: Co-occurring woody species have diverse hydraulic strategies and mortality rates during an extreme drought. – Plant Cell Environ. **41**: 576-588, 2018b.

Klemm T., Briske D.D., Reeves M.C.: Vulnerability of rangeland beef cattle production to climate-induced NPP fluctuations in the US Great Plains. – Glob. Change Biol. **26**: 4841-4853, 2020.

Knief U., Forstmeier W.: Violating the normality assumption may be the lesser of two evils. – Behav. Res. Method. **53**: 2576-2590, 2021.

Lazár D.: Parameters of photosynthetic energy partitioning. – J. Plant Physiol. **175**: 131-147, 2015.

Lenth R.V., Buerkner P., Herve M. *et al.*: Package '*emmeans*'. R package version 1.4-8. *Available at*: https://cran.r-project.org/web/packages/emmeans/index.html, 2020.

Lichtenthaler H.K.: Chlorophyll and carotenoids: Pigments of biosynthetic compounds. – Method. Enzymol. **148**: 350-382, 1987.

Liu N., Guan L.: Linkages between woody plant proliferation dynamics and plant physiological traits in southwestern North America. – J. Plant Ecol. **5**: 407-416, 2012.

Lombardini L., Rossi L.: Ecophysiology of plants in dry environments. – In: D'Odorico P., Porporato A., Wilkinson Runyan C. (ed.): Dryland Ecohydrology. Pp. 71-100. Springer, Cham 2019.

Loriaux S.D., Avenson T.J., Welles J.M. *et al.*: Closing in on maximum yield of chlorophyll fluorescence using a single multiphase flash of sub-saturating intensity. – Plant Cell Environ. **36**: 1755-1770, 2013.

Malnoë A.: Photoinhibition or photoprotection of photosynthesis? Update on the (newly termed) sustained quenching component qH. – Environ. Exp. Bot. **154**: 123-133, 2018.

Martínez-Ferri E., Balaguer L., Valladares F. *et al.*: Energy dissipation in drought-avoiding and drought-tolerant tree species at midday during the Mediterranean summer. – Tree Physiol. **20**: 131-138, 2000.

Maxwell K., Johnson G.N.: Chlorophyll fluorescence – a practical guide. – J. Exp. Bot. **51**: 659-668, 2000.

McElrone A.J., Pockman W.T., Martinez-Vilalta J., Jackson R.B.: Variation in xylem structure and function in stems and roots of trees to 20 m depth. – New Phytol. **163**: 507-517, 2004.

Meyer R.E., Morton H.L., Haas R.H. *et al.*: Morphology and anatomy of honey mesquite. Technical Bulletin No. 1423. Pp. 190. Agricultural Research Service, USDA, Washington 1971.

Míguez F., Fernández-Marín B., Becerril J.M., García-Plazaola J.I.: Activation of photoprotective winter photoinhibition in plants from different environments: A literature compilation and meta-analysis. – Physiol. Plantarum **155**: 414-423, 2015.

Moore G.W., Edgar C.B., Vogel J.G. *et al.*: Tree mortality from an exceptional drought spanning mesic to semiarid ecoregions. – Ecol. Appl. **26**: 602-611, 2016.

Msanne J., Awada T., Bryan N.M. *et al.*: Ecophysiological responses of native invasive woody *Juniperus virginiana* L. to resource availability and stand characteristics in the semiarid grasslands of the Nebraska Sandhills. – Photosynthetica **55**: 219-230, 2017.

Müller P., Li X.P., Niyogi K.K.: Non-photochemical quenching. A response to excess light energy. – Plant Physiol. **125**: 1558-1566, 2001.

Murchie E.H., Lawson T.: Chlorophyll fluorescence analysis: A guide to good practice and understanding some new applications. – J. Exp. Bot. **64**: 3983-3998, 2013.

Murchie E.H., Ruban A.V.: Dynamic non-photochemical quenching in plants: from molecular mechanism to productivity. – Plant J. **101**: 885-896, 2020.

Owens M.K.: The role of leaf and canopy-level gas exchange in the replacement of *Quercus virginiana* (Fagaceae) by *Juniperus ashei* (Cupressaceae) in semiarid savannas. – Am. J. Bot. **83**: 617-623, 1996.

Owens M.K., Schreiber M.C.: Seasonal gas exchange characteristics of two evergreen trees in a semiarid environment. – Photosynthetica **26**: 389-398, 1992.

Pinheiro J.C., Bates D.M.: Mixed-effects models in S and S-PLUS. Pp. 528. Springer, New York 2000.

Pinheiro J., Bates D., DebRoy S. *et al.*: *nlme*: Linear and Nonlinear Mixed Effects Models. R package version 3.1-148. *Available at*: https://CRAN.R-project.org/package=nlme, 2020.

Poulter B., Frank D., Ciais P. *et al.*: Contribution of semi-arid ecosystems to interannual variability of the global carbon cycle. – Nature **509**: 600-603, 2014.

Schielzeth H., Dingemanse N.J., Nakagawa S. *et al.*: Robustness of linear mixed-effects models to violations of distributional assumptions. – Method. Ecol. Evol. **11**: 1141-1152, 2020.

Seager R., Feldman J., Lis N. *et al.*: Whither the 100th meridian? The once and future physical and human geography of America's arid–humid divide. Part II: The meridian moves East. – Earth Interact. **22**: 1-24, 2018.

Seager R., Ting M., Held I. *et al.*: Model projections of an imminent transition to a more arid climate in Southwestern North America. – Science **316**: 1181-1184, 2007.

Sims D.A., Gamon J.A.: Relationships between leaf pigment content and spectral reflectance across a wide range of species, leaf structures and developmental stages. – Remote Sens. Environ. **81**: 337-354, 2002.

Strzepek K., Yohe G., Neumann J., Boehlert B.: Characterizing changes in drought risk for the United States from climate change. – Environ. Res. Lett. **5**: 044012, 2010.

Thurow T.L., Hester J.W.: Holistic perspective, rangeland hydrology and wildlife considerations in juniper management: How an increase or reduction in juniper cover alters rangeland hydrology. – In: Taylor C.A. (ed.): Proceedings of 1997 Juniper Symposium, Texas Agricultural Experiment Station Technical Report 97-1. Pp. 9-22. Texas A&M University Research and Extension Center, Sonora 1997.

Thyroff E.C., Burney O.T., Mickelbart M.V., Jacobs D.F.: Unraveling shade tolerance and plasticity of semi-evergreen oaks: Insights from maritime forest live oak restoration. – Front. Plant Sci. **10**: 1526, 2019.

Turner N.C.: Measurement of plant water status by the pressure chamber technique. – Irrigation Sci. **9**: 289-308, 1988.

Van Auken O.W.: Causes and consequences of woody plant encroachment into western North American grasslands. – J. Environ. Manage. **90**: 2931-2942, 2009.

Verhoeven A.: Sustained energy dissipation in winter evergreens. – New Phytol. **201**: 57-65, 2014.

Verhoeven A., García-Plazaola J.I., Fernández-Marín B.: Shared mechanisms of photoprotection in photosynthetic organisms tolerant to desiccation or to low temperature. – Environ. Exp. Bot. **154**: 66-79, 2018.

Wei L., Xu C., Jansen S. *et al.*: A heuristic classification of woody plants based on contrasting shade and drought strategies. – Tree Physiol. **39**: 767-781, 2019.

Wellburn A.R.: The spectral determinations of chlorophylls *a* and *b*, as well as total carotenoids, using various solvents with spectrophotometers of different resolutions. – J. Plant Physiol. **144**: 307-313, 1994.

Werner C., Correia O., Beyschlag W.: Characteristic patterns of chronic and dynamic photoinhibition of different functional groups in a Mediterranean ecosystem. – Funct. Plant Biol. **29**: 999-1011, 2002.

Western Regional Climate Center (WRCC).: Sonora, TX: Total of precipitation (inches). *Available at*: https://wrcc.dri.edu/cgi-bin/cliMAIN.pl?tx8449, 2020.

Wilson T.B., Webb R.H., Thompson T.L.: Mechanisms of range expansion and removal of mesquite in desert grasslands of the Southwestern United States. Rocky Mountain Research Station General Technical Report 81. Pp. 28. U.S. Department of Agriculture, Forest Service, 2001.